AIP | Physics of Plasmas

Ion cyclotron resonance frequency heating in JET during initial operations with the ITER-like walla)

P. Jacquet, V. Bobkov, L. Colas, A. Czarnecka, E. Lerche, M.-L. Mayoral, I. Monakhov, D. Van-Eester, G. Arnoux, S. Brezinsek, M. Brix, A.-L. Campergue, S. Devaux, P. Drewelow, M. Graham, C. C. Klepper, A. Meigs, D. Milanesio, J. Mlynar, T. Pütterich, A. Sirinelli, and JET-EFDA Contributors

Citation: Physics of Plasmas (1994-present) **21**, 061510 (2014); doi: 10.1063/1.4884354
View online: http://dx.doi.org/10.1063/1.4884354
View Table of Contents: http://scitation.aip.org/content/aip/journal/pop/21/6?ver=pdfcov
Published by the AIP Publishing

Ion cyclotron resonance frequency heating in JET during initial operations with the ITER-like wall[a)]

P. Jacquet,[1,b)] V. Bobkov,[2] L. Colas,[3] A. Czarnecka,[4] E. Lerche,[5] M.-L. Mayoral,[1,6] I. Monakhov,[1] D. Van-Eester,[5] G. Arnoux,[1] S. Brezinsek,[7] M. Brix,[1] A.-L. Campergue,[8] S. Devaux,[2] P. Drewelow,[2] M. Graham,[1] C. C. Klepper,[9] A. Meigs,[1] D. Milanesio,[10] J. Mlynar,[11] T. Pütterich,[2] A. Sirinelli,[1] and JET-EFDA Contributors[12,c)]
[1]*Euratom/CCFE Fusion Association, Culham Science Centre, Abingdon OX14 3DB, United Kingdom*
[2]*Max-Planck-Institut für Plasmaphysik, EURATOM-Assoziation, Garching, Germany*
[3]*CEA, IRFM, F-13108 Saint-Paul-Lez-Durance, France*
[4]*Association Euratom-IPPLM, Hery 23, 01-497 Warsaw, Poland*
[5]*Association EURATOM-Belgian State, ERM-KMS, Brussels, Belgium*
[6]*EFDA Close Support Unit, Garching, Germany*
[7]*IEK-4, Forschungszentrum Jülich, Association EURATOM-FZJ, Jülich, Germany*
[8]*Ecole Nationale des Ponts et Chaussées, F77455 Marne-la-Vallée, France*
[9]*Oak Ridge National Laboratory, Oak Ridge, Tennessee 37831-6169, USA*
[10]*Politecnico di Torino, Department of Electronics, Torino, Italy*
[11]*Association EURATOM-IPP.CR, Za Slovankou 3, 182 21 Praha 8, Czech Republic*
[12]*JET-EFDA, Culham Science Centre, Abingdon OX14 3DB, United Kingdom*

(Received 15 November 2013; accepted 10 February 2014; published online 24 June 2014)

In 2011/12, JET started operation with its new ITER-Like Wall (ILW) made of a tungsten (W) divertor and a beryllium (Be) main chamber wall. The impact of the new wall materials on the JET Ion Cyclotron Resonance Frequency (ICRF) operation is assessed and some important properties of JET plasmas heated with ICRF are highlighted. A $\sim 20\%$ reduction of the antenna coupling resistance is observed with the ILW as compared with the JET carbon (JET-C) wall. Heat-fluxes on the protecting limiters close the antennas, quantified using Infra-Red thermography (maximum 4.5 MW/m^2 in current drive phasing), are within the wall power load handling capabilities. A simple RF sheath rectification model using the antenna near-fields calculated with the TOPICA code can reproduce the heat-flux pattern around the antennas. ICRF heating results in larger tungsten and nickel (Ni) contents in the plasma and in a larger core radiation when compared to Neutral Beam Injection (NBI) heating. The location of the tungsten ICRF specific source could not be identified but some experimental observations indicate that main-chamber W components could be an important impurity source: for example, the divertor W influx deduced from spectroscopy is comparable when using RF or NBI at same power and comparable divertor conditions, and Be evaporation in the main chamber results in a strong reduction of the impurity level. In L-mode plasmas, the ICRF specific high-Z impurity content decreased when operating at higher plasma density and when increasing the hydrogen concentration from 5% to 15%. Despite the higher plasma bulk radiation, ICRF exhibited overall good plasma heating performance; the power is typically deposited at the plasma centre while the radiation is mainly from the outer part of the plasma bulk. Application of ICRF heating in H-mode plasmas has started, and the beneficial effect of ICRF central electron heating to prevent W accumulation in the plasma core has been observed. [http://dx.doi.org/10.1063/1.4884354]

I. INTRODUCTION

In 2011/12, JET started operation with its new ITER-Like Wall (ILW)[1] made of a tungsten divertor and a beryllium main chamber wall with some recessed W-coated components (e.g., Neutral Beam Injection (NBI) shine-through protection tiles, re-ionisation tiles, restraint ring protections). Ion Cyclotron Resonance Frequency (ICRF) heating using the A2 antennas[2] was routinely used to provide central electron heating in support to the experimental program which focused on the characterization of fuel retention with the ILW, characterization of H-mode access and high performance scenario development.[3] Plasma compatibility and performance of ICRF heating (hydrogen minority, deuterium plasma) with the full metallic environment was studied;[4] 5 MW of RF power were launched into L-mode plasmas and up to 4 MW in ELMy H-mode. The main objectives of the initial ICRF experiments in JET with the ILW (JET-ILW) was to verify compatibility of the operation with the ILW environment: (a) Verify if the new wall induced a change in the antenna coupling resistance. (b) Characterize ICRF specific heat loads on the Plasma Facing Components

[a)]Invited contribution to the 20th AIP conference on RF power in plasma, 25-28 June 2013, Sorrento, Italy.
[b)]Author to whom correspondence should be addressed. Electronic mail: philippe.jacquet@ccfe.ac.uk
[c)]See the Appendix of F. Romanelli *et al.*, Proceedings of the 24th IAEA Fusion Energy Conference, 2012, San Diego, USA.

(PFCs) in the vicinity of the antennas. (c) Verify if the use of ICRF with the ILW led to an increased level of W impurity in the plasma. (d) Characterize JET plasmas with ICRF heating, from the point of view of heating performance (the increase of total plasma energy per applied unit of ICRF power) and of the effect of central heating on high Z impurity transport.

The JET ICRF heating system includes four "A2" ICRF antennas (A, B, C, and D, see Figure 1). The ITER-Like ICRF antenna (ILA) was not used in 2011/12. Each A2 antenna[2,5,6] is a phased array of 4 poloidal straps; controlling the phase between straps allows waves to be launched with different $k_{//}$ spectra. Usually $[0,\pi,0,\pi]$ (π phasing), $[0,\pi/2,\pi,-\pi/2]$ ($+\pi/2$ phasing) or $[0,-\pi/2,\pi,\pi/2]$ ($-\pi/2$ phasing) phasing conditions are applied to straps [1,2,3,4]. The plasma facing part of the antennas is covered by a Faraday screen consisting of tilted solid Be rods. Each antenna is surrounded by two poloidal limiters made of solid Be tiles, and a vertical septum made of solid Be is fitted at the centre of each antenna. The feeding configuration of antenna A and B during the initial campaign with the ILW was slightly different than the usual arrangement (see Figure 2): Straps 1 and 2 of antennas A and B were fed by the same RF amplifiers through a 3 dB hybrid coupler system[5] also providing ELM resilience. Straps 3 and 4 of antenna A were fed by independent amplifiers. Straps 3 and 4 of antenna B could not be powered, consequently only straps 1,2 of antenna A and B could be used on ELMy H-mode plasmas. A numerical model of the A2 antennas has recently been built to be used with the antenna electromagnetic modeling code TOPICA[7] (see Figure 3), the same antenna code is used for the design of the ITER ICRF antenna.[8] TOPICA simulations are now being used to analyze the operation of JET A2 antennas.

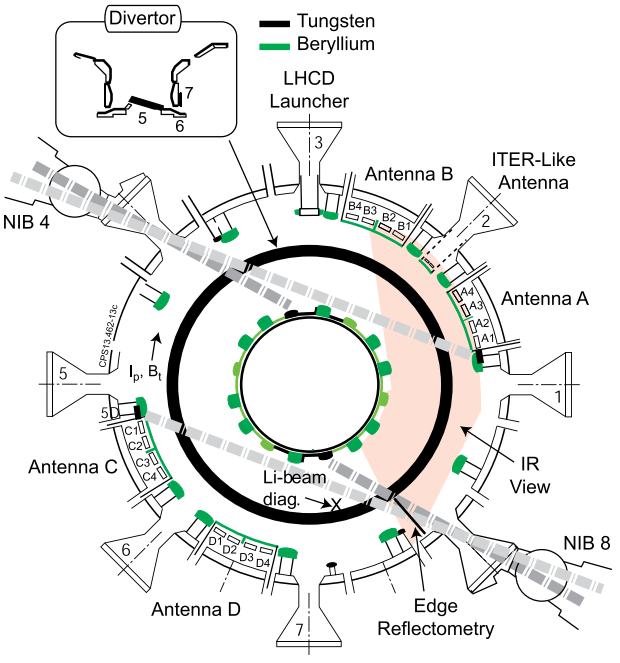

FIG. 1. Top view of JET, showing the JET ICRF antennas (A, B, C, D). The view from the IR camera looking at antenna A and B is indicated. Also shown is the position of the reflectometry (located at the mid-plane) and Lithium-beam (located at the top) SOL diagnostics. Elements with tungsten surfaces are in black.

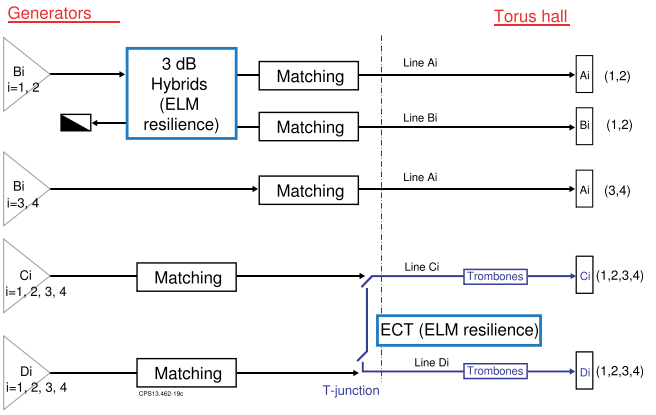

FIG. 2. ICRF antennas feeding configuration during the initial campaign with the JET–ILW (2011–2012).

II. ANTENNAS OPERATION AND RF/SOL INTERACTION

A. Antenna loading

For a given V_{max}, the maximum operating RF voltage in the antenna structure (or in the ICRF system transmission lines) limited by voltage stand-off, the achievable coupled power varies to a first approximation linearly with the antenna coupling resistance R_c: $P_{coupled} \sim V_{\max}^2 R_c / 2 Z_c^2$, where Z_c is the transmission line characteristic impedance ($Z_c = 30\ \Omega$ for JET ICRF transmission lines). The antenna coupling resistance Rc is expected to decrease exponentially with the distance between the antenna and the fast wave density cut-off position,[9] the cut-off density being typically in the range of $1\text{–}5 \times 10^{18}\ \mathrm{m}^{-3}$ for JET operating parameters. A statistical analysis of Rc has been carried-out to verify whether if the change to a low recycling wall (the ILW) has led to changes in the Scrappe-Off Layer (SOL) properties which affect the ICRF antenna coupling resistance. The result is shown in Figure 4 for antenna A. Rc is plotted as a

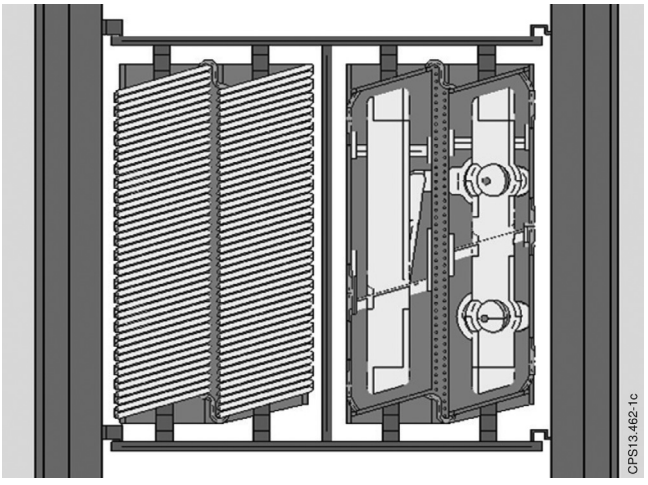

FIG. 3. Representation of the JET A2 Antenna TOPICA model. The screen bars were removed from the model representation on the right to illustrate the strap geometry.

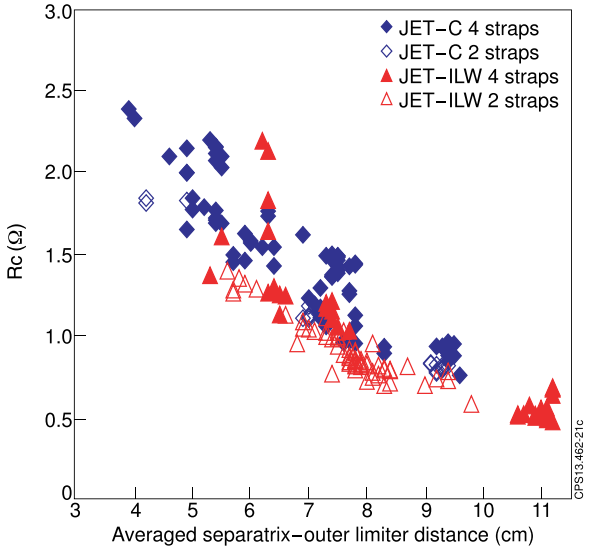

FIG. 4. For antenna A, the coupling resistance is plotted as a function of the averaged separatrix–outer limiter distance over the height of the antenna straps. The data set includes JET-C and JET-ILW plasmas with low triangularity, and line integrated density in the range of 5–6.5 × 10^{19} m^{-2}. Antenna phasing is π, and the operating frequency is 42.56 MHz. Operation with all 4 antenna straps are represented with solid symbols (data from the 2013 restart with the JET-ILW are included), operation with straps 1 and 2 only are represented with open symbols.

function of the averaged plasma-outer limiter distance over the antenna straps height. The data set includes L-mode pulses with low triangularity, B_T in the range of 2.35–2.9 Tesla, I_P in the range of 1.8–2.5 MA; the line integrated density is in the range of 5–6.5 × 10^{19} m^{-2}. The operating frequency is 42.56 MHz and the strap phasing is π. The coupling resistance is averaged over the operating straps. One can note that the coupling resistance decreases approximately exponentially with the plasma-outer limiter distance as expected. The scatter in the JET-C data is larger, this is attributed to the fact that the JET-C data-set includes pulses with a wider range of operating conditions that can affect the SOL conditions, in particular, different divertor configurations with the outer strike point either on tile 5, 6 or 7 (see Figure 1). On the contrary, the JET-ILW dataset includes almost exclusively plasmas with the strike point on tile 5.

For equivalent plasma outer limiter distance, plasma shape and plasma density, the A2 antennas coupling resistance in JET-ILW is slightly reduced (by ∼20% at most) as compared with JET-C, which is equivalent to an inward shift of the cut-off layer of ∼1 cm; this could be a consequence from the change in the wall recycling properties, although no obvious differences were observed comparing JET-C and JET-ILW SOL measurements.[10] The slightly improved coupling with the JET-C could be a consequence of local changes in the SOL properties in front of the powered antennas from the local recycled gas as was observed in ICRF coupling improvement via local gas puffing experiments in ASDEX-Upgrade[11] and JET.[12] Finally one could not rule out the possible introduction of a systematic error of the order of 1 cm in the localization of the separatrix position from plasma equilibrium reconstruction when going from JET-C to JET-ILW.

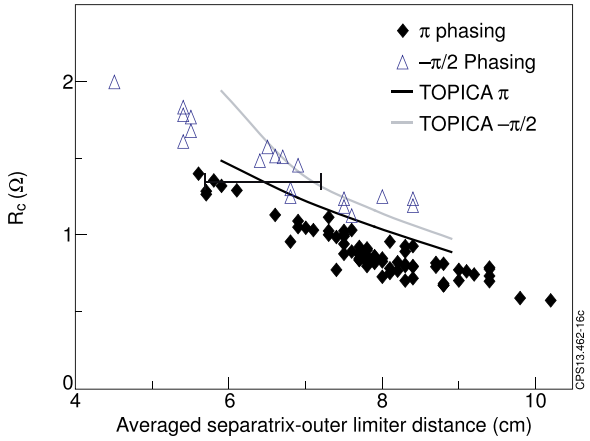

FIG. 5. Antenna A coupling resistance measured in JET-ILW and results from TOPICA simulations. Only straps 1 and 2 are powered. The data set includes plasmas of similar shapes with line integrated density in the range of 5–6.5 × 10^{19} m^{-2}.

Preliminary results for the analysis of the A2 antennas *Rc* measurements using TOPICA are presented in Figure 5. For a series of JET-ILW L-mode pulses where the plasma mid-plane outer gap was changed, *Rc* from antenna A is compared to the calculations from TOPICA; in these cases only straps 1 and 2 were used. The plasma temperature and density profiles representative of the profiles in the L-mode discharges have been loaded in TOPICA simulations. For π phasing, the simulations reproduce well the measured coupling resistance dependence with antenna-plasma distance. For $-\pi/2$ phasing, the measured coupling resistance is higher as compared to π phasing, this behavior is also reproduced in TOPICA simulations. The error bar in Figure 5 corresponds to the uncertainty in the absolute radial position of the SOL density profiles measured in JET (from the reflectometry diagnostic or Lithium-beam diagnostic). Further analysis is ongoing to study cases with the 4 antenna straps powered, providing a further and sound validation of this numerical tool.

B. ICRF specific heat loads on antenna limiters

When using ICRF heating, local hot spots from enhanced heat-fluxes are commonly observed on some plasma facing components close to the antennas,[13] an example is shown in Figure 6. Experiments have been carried out during the initial experimental campaign with the JET-ILW to characterize the heat flux to the A2 antenna limiters.[14] Using Infra-Red (IR) thermography and thermal models of the tiles, heat-fluxes were evaluated from the surface temperature increase during the RF phase of L-mode plasmas. The maximum observed heat-flux intensity was ∼4.5 MW/m^2, observed on antenna A when operating with the 4 straps; the strap phasing was $-\pi/2$, the power was 2 MW on antenna A, and the plasma midplane outer gap was 4 cm. The surface temperature increase was $\Delta T_{surface} = 375\,^{\circ}C$ on antenna A septum during the 5 s ICRF phase (JET pulse Nb 81702). The heat-fluxes were enhanced when using current drive phasing; the intensity was found to increase linearly with the density at radial position corresponding to the antenna and with V_{RF}^2, the square of the RF voltage at the antinodes of the

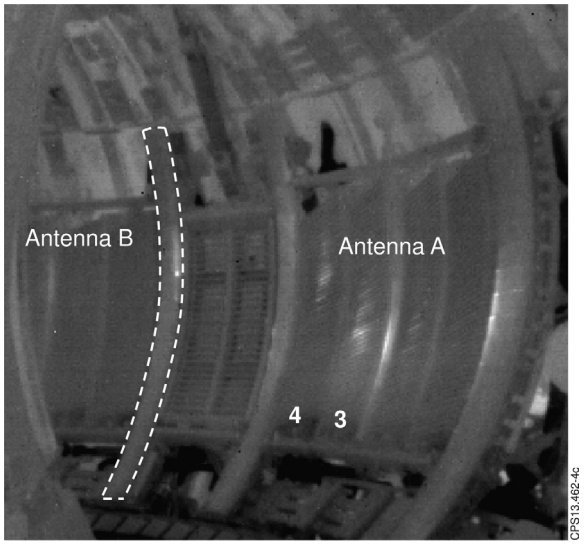

FIG. 6. Pulse 83063 t = 13.0 s, IR camera frame showing ICRF hot spots when antenna A (straps 3,4) is powered. The heat-flux on the limiter highlighted with dotted lines is analyzed in Figure 8.

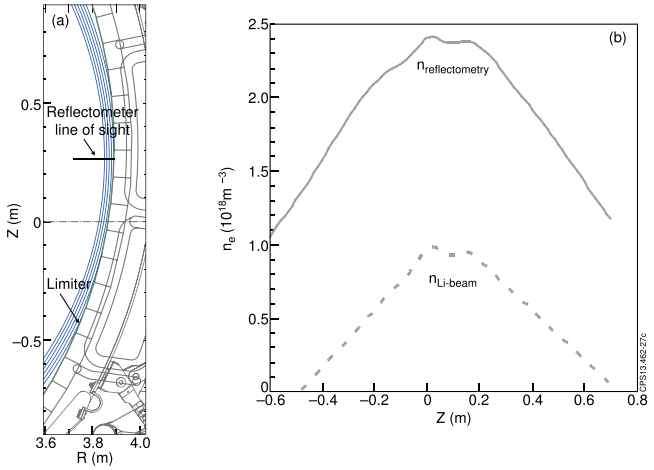

FIG. 7. (a) 2D poloidal cross section of field lines in the SOL and of an antenna poloidal limiter (pulse 83063, t = 13.0 s). The reflectometry line of sight is shown. The Li-beam diagnostic line of sight is at the top of the plasma, at R = 3.25 m (not shown). (b) Reflectometry and Li-beam electron density measurements mapped along the antenna limiter.

transmission lines feeding the antenna. The Be tiles of the A2s protecting limiters can handle fluxes of the order of 6 MW/m^2 for 10 s, therefore, RF specific heat-fluxes are in practice not a limitation for JET ICRF operation (although hot spots need to be monitored). However, these heat-flux values deserve further attention, in particular, when compared to the engineering design targets (5 MW/m^2) for the ITER ICRF antenna Faraday screen and neighboring blanket modules.

To optimize the design of the antennas for future devices, modeling activities of ICRF sheath rectification are carried out within the ICRF community (see, for example, Ref. 15). We have tested a simple RF sheath rectification model, in particular, to verify if the intensity and the location of the hot-spots measured on the JET antenna protecting limiters is consistent with the $E_{//}$ map in front of the A2s as calculated using the TOPICA code ($E_{//}$ is the RF electric field that drive RF sheath rectification, // denotes the direction parallel to static magnetic field).[16] In the simplified model derived from Ref. 17, $Q_{//} = e Z n c_s V_{DC}$ where e is the elementary charge, Z is the atomic number of plasma ions (D_+), c_s is the ion sound speed in the SOL, n is the electron density at the antenna and $V_{DC} = \frac{1}{\pi}|\int E_{//} dl|$ is the RF rectified sheath potential. In the model, the reflectometer or lithium-beam density measurements are mapped along the poloidal limiters to estimate the local density. Figure 7 illustrates this procedure: in the poloidal plane, the outer plasma radius of curvature is smaller than the antenna limiter radius, hence points along the vertical direction on the limiter lay on different flux surfaces; points located at the top and at the bottom of the limiter are further away from the plasma separatrix, the density at these locations is smaller than at the plasma midplane. The SOL density measurements from the reflectometry diagnostic and the Li-beam diagnostic are mapped on the poloidal limiter using flux surface reconstruction based on the EFIT equilibrium code.[18] The $E_{//}$ field in front of the antenna is from TOPICA modeling. The field is calculated 4.5 mm in front of the limiters; the field intensity is scaled to the launched ICRF power. The integration path to calculate V_{DC} is along the tilted field lines up until the location of the poloidal limiter. A typical result is shown in Figure 8 for pulse 83063 where only strap 3 and 4 of antenna A were used with $-\pi/2$ phasing. The heat-flux estimated from IR thermography along the 2D poloidal limiter is plotted as a function of the vertical position, and it is compared to the estimates from the simple model; the model can reproduce the vertical location of the maximum heat-flux and the magnitude of the heat-flux within the uncertainty of the density measurements. It is important to take into account the variation of n along the height of the limiter (plasma-limiter distance is not uniform along the limiter, n peaks at ~0.3 m) in order for the model to reproduce the location of the maximum load. The model is also consistent with the observed reduced intensity of the hot-spot when the strap phasing is π instead of current drive. However, the simple model cannot

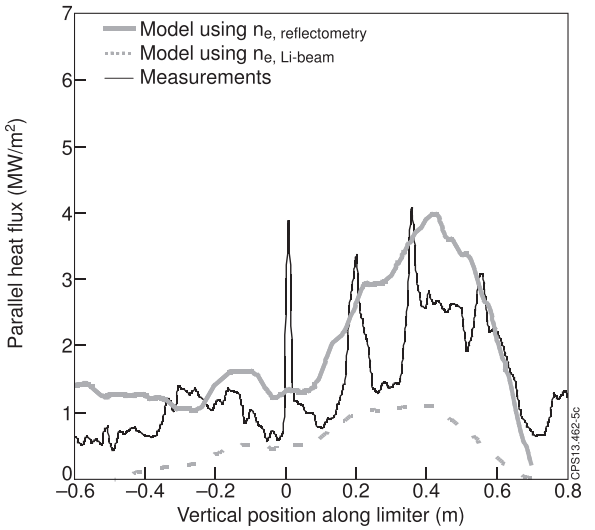

FIG. 8. Pulse 83603, t = 13 s, comparison between the heat-flux measured along the poloidal limiter and results from the simple model.

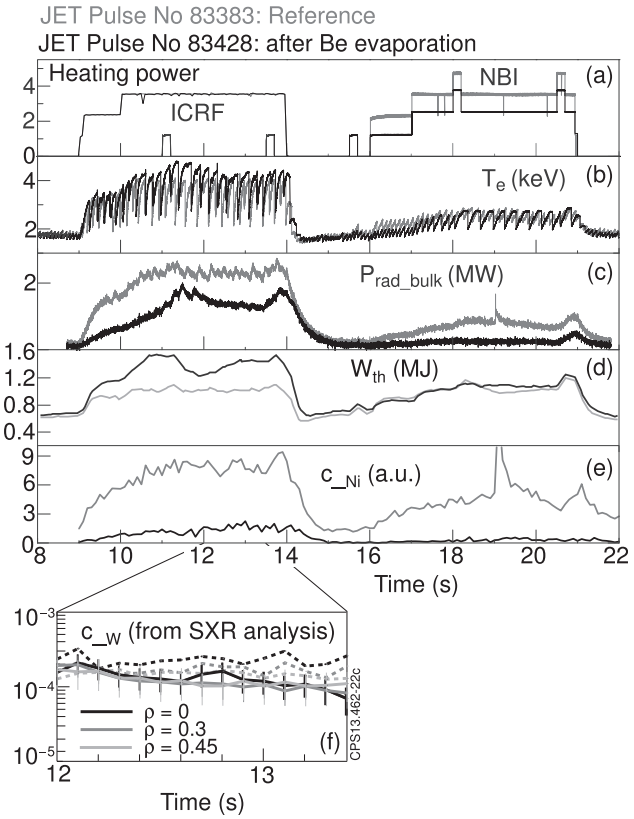

FIG. 9. For pulse 83383 (before Be evaporation, in grey) and 83428 (after evaporation, in black) time trace of (a) ICRF and NBI power, (b) Te at plasma centre, (c) core radiated power from bolometry, (d) plasma thermal energy (obtained subtracting the RF and NBI fast ion contributions to the MHD energy evaluated using magnetic measurements and equilibrium reconstruction code), and (e) Ni concentration evaluated from VUV spectroscopy. In (f), W concentration evaluated from SXR analysis at different normalized radius is shown (83383 with dashed lines).

explain the observed experimental scaling of the ICRF specific heat-loads with V_{RF}^2, more complex phenomena such as the modification of plasma properties in front of the antennas by ICRF power can also be involved explaining this scaling.[19]

C. ICRF specific impurity source

During ICRF heating, the bulk radiated power is found to increase compared to C-wall operation although not preventing effective heating of the plasma (see Section III B). The main radiators in the plasma bulk are W (new to the JET-ILW) and Ni which was also observed in JET-C,[20] the increased level of radiation in the JET-ILW plasmas being attributed to the tungsten. The radiated power is noticeably higher when using ICRF instead of NBI heating (see Figures 9, 10, and 12). The plasma Be content is also higher with ICRF heating.

Ni (Ref. 20) and W (Refs. 21 and 22) were detected from Vacuum Ultra Violet (VUV) spectroscopy operating in the range of 10–110 nm. Analysis of Soft-X Ray (SXR) signals including a 2D spatial deconvolution of the emission was also used to evaluate the W concentration (c_W) profiles[21] in the plasma. In this case, the Bremstrahlung emission from low Z impurities is subtracted from the SXR signals and it is assumed that W is the only other radiator contributing to SXR emission. Further, the total radiation profiles can be recalculated and compared to the Bolometric measurements (Figure 13).

One could invoke a change in transport of W and Ni in the plasma core during ICRF to explain the enhanced level of impurity when using ICRF, but preliminary transport analysis[23] suggests that there are also specific ICRF Ni and W sources. It was plausible to suspect that RF sheath rectification along the field lines which connect the powered antennas to the divertor, could enhance W sputtering in the divertor region. ICRF field–SOL interaction could indeed be evidenced;[24] For example, enhanced Be sputtering was observed using Be I or Be II line spectroscopy with line of sight falling on a limiter close to antenna D or on the Faraday Screen in front of strap 4 of antenna D.[25] The effect was enhanced when using $-\pi/2$ strap phasing. Also, the W I emission at the outer divertor baffles, measured with an intensified CCD camera fitted with a 1 nm filter (centered at 400.9 nm), was found to change depending on which specific antenna was powered, the effect in this case also increased when using $-\pi/2$ phasing which is expected to generate higher V_{DC} that drives RF sheath rectification. The possible mechanisms responsible for enhanced sputtering of W and Ni during RF are: (a) near field RF sheath rectification; (b) far field RF sheath rectification; (c) charge exchanged neutrals of RF accelerated fast particles. However, we could not identify the main mechanism at play in JET and we could not directly link the increased W content in the plasma to a specific W source when using ICRF heating. In particular, W

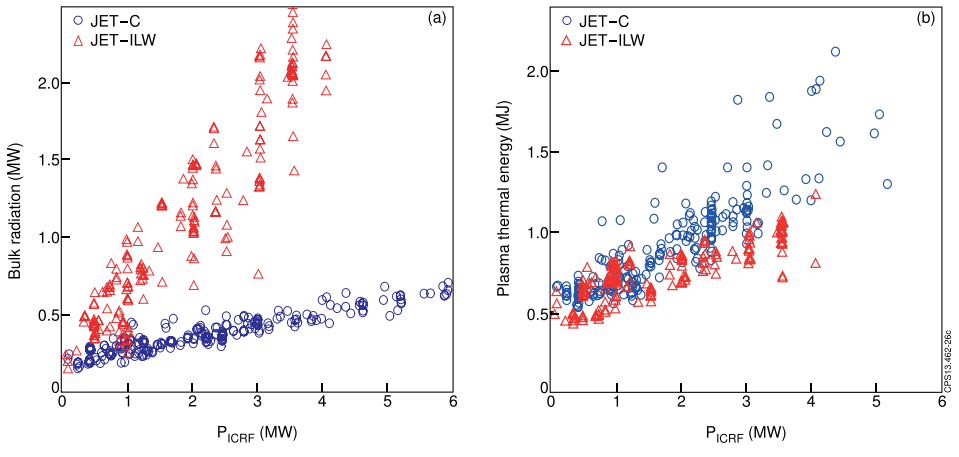

FIG. 10. For a database of JET-C and JET-ILW L-mode ICRF heated plasmas, comparison of: (a) power radiated from bulk plasma, from bolometry diagnostic; (b) plasma thermal energy evaluated from the High-Resolution Thomson diagnostic assuming equal electron and ion temperatures. The database includes pulses with ICRF frequency = 42 MHz, π antenna strap phasing, $2.5\,T < B_T < 2.8\,T$ (central heating), $1.8MA < I_P < 2.5MA$, line integrated density in the range of $5–7 \times 10^{19} m^{-2}$.

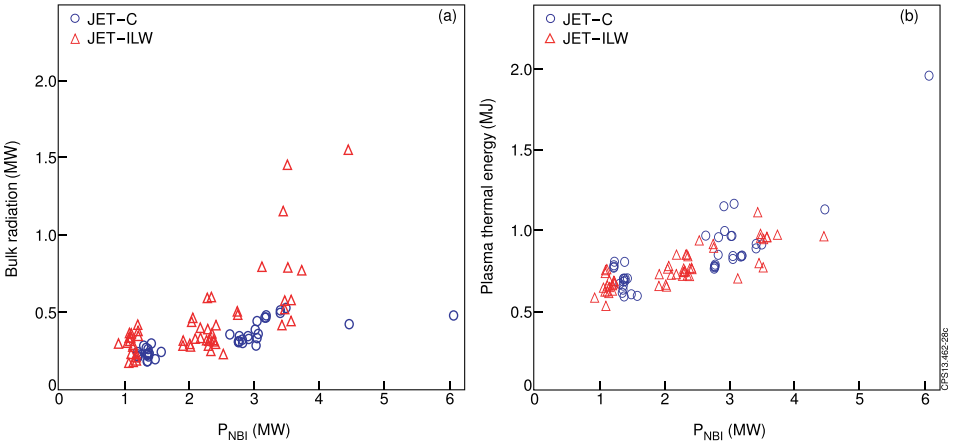

FIG. 11. For a database of JET-C and JET-ILW L-mode NBI heated plasmas, comparison of: (a) power radiated from bulk plasma, from bolometry diagnostic; (b) plasma thermal energy evaluated from the High-Resolution Thomson diagnostic assuming equal electron and ion temperatures. The database includes pulses $2.4T < B_T < 2.8\,T$, $1.8MA < I_P < 2.5MA$, line integrated density in the range of $5–7 \times 10^{19} m^{-2}$.

line emission spectroscopy[26] did not evidence higher W sputtering in the divertor region when using ICRF heating.[24] The W components located in the main chamber could also contribute importantly to the W in the plasma. In limiter configuration, ICRF heated plasmas also had higher c_W compared to NBI. Moreover, when in such a limiter discharge the plasma was shifted upwards away from the divertor, providing better magnetic isolation between the divertor and the antennas, c_W did not decrease. Further, we have investigated the effect of covering the wall with a thin layer of Be through an overnight evaporation (see Figure 9). Comparison of reference pulses before/after evaporation (~3 nm thick Be layer) shows a strong reduction of the Ni and W concentration level, and of the bulk radiated power. Also observed is an increase of the thermal energy after Be evaporation (Figure 9(d)). The effect of Be evaporation on plasma radiation was still visible when repeating the reference pulse after ~10 ELMy H-modes pulses. This is consistent with the idea that Ni and W surfaces on remote areas in the main chambers were screened from sputtering by the Be layer which suggests that these areas contribute significantly to the high Z impurity source in JET.

III. ICRF PLASMA HEATING

A. Plasma parameters and high Z impurity content

For ICRF and NBI heated plasmas, the edge density is a key parameter that influences the plasma impurity content, c_W (Ref. 24) and c_{Ni} (Ref. 22) being both reduced when operating at higher density. A number of different processes could lead to this result: (a) a decrease of the impurity source from a reduced electron temperature in the SOL when operation at higher density (using higher level of gas dosing); (b) a change in impurity transport properties; (c) a direct dilution of the impurities in the plasma; and (d) in the case of ICRF, a reduction of the antenna RF field at higher SOL density reducing RF sheath rectification effects.

An experiment was run to investigate the effect of the hydrogen minority concentration on impurity concentration in L-mode plasmas ($B_T = 2.7$ T, $I_P = 2$MA, 42 MHz ICRF); working at H concentration of ~15%—somewhat higher than the few percents traditionally used for minority heating—caused a reduction of the W and Ni concentration and of the bulk radiation. Impurity concentration and radiated power increased again when the H fraction was increased above 20%. A tentative explanation for these observations has been proposed in Ref. 27: increasing the hydrogen fraction on one hand increased the edge density; As already mentioned in the previous paragraph, this tends to reduce the plasma impurity content. But it also reduced the wave absorption efficiency in the plasma core which increased the power fraction re-incident on the edge, the latter hindering coupling when the hydrogen fraction was increased above 20%. We should also add that for the pulses with low H

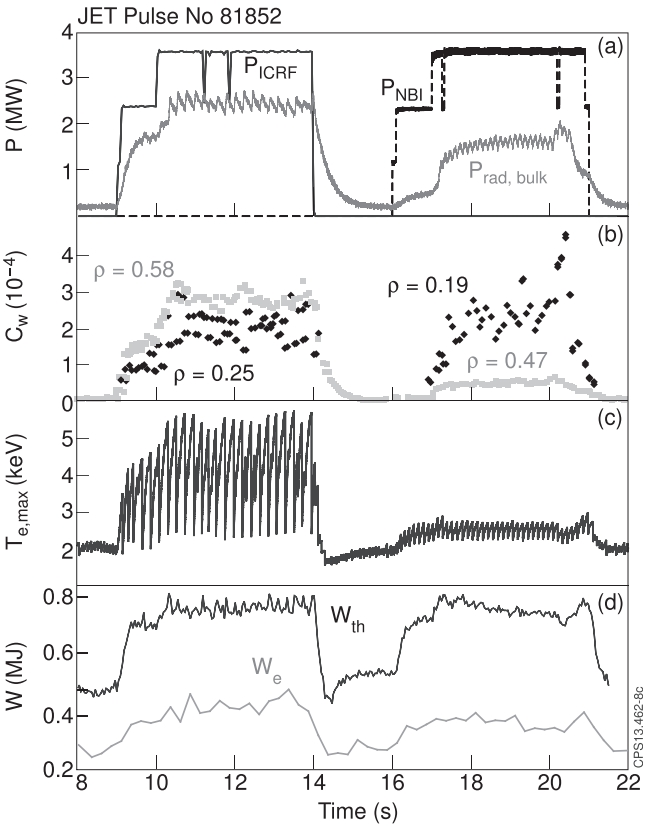

FIG. 12. For pulse 81852, (a) time trace of ICRF and NBI power and power radiated in the core plasma (grey line); (b) W concentration evaluated by VUV spectroscopy, ρ is the normalized radius, (c) central electron temperature; (d) W_{th}, thermal energy (obtained subtracting the RF and NBI fast ion contributions to the MHD energy evaluated using magnetic measurements and equilibrium reconstruction code) and W_e, electron energy content (evaluated from High-Resolution Thomson Scattering diagnostic).

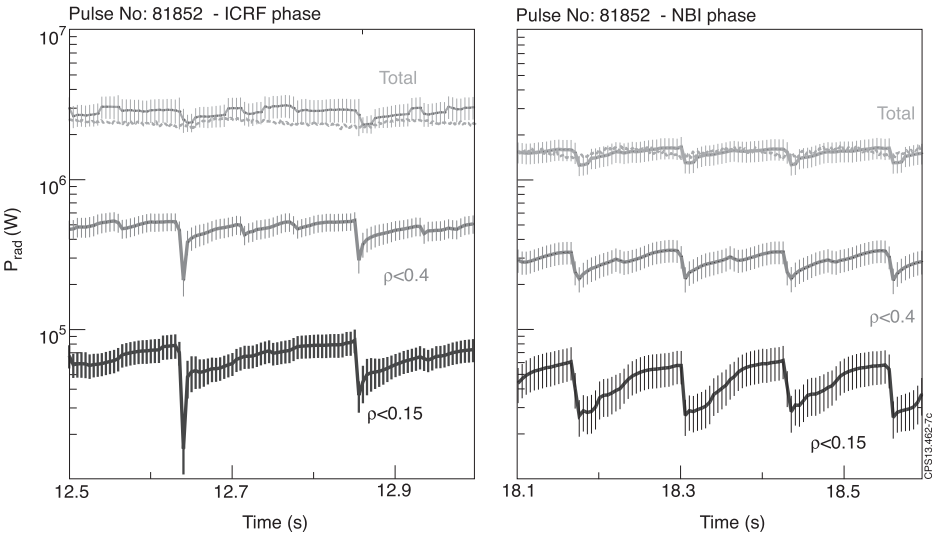

FIG. 13. Radiated power (from bolometry and SXR analysis) during the ICRF and NBI phase for pulse 81852; total from plasma bulk (light grey), radiated inside normalized radius (ρ) of 0.4 (grey), and inside $\rho = 0.15$ (black).

concentration, the plasma entered into M-mode (regime with enhanced particle confinement[28]); this change in confinement regime could be involved in the observed changes in the SOL density when varying the H fraction. The effect of the M-mode of the high Z impurity transport at the edge barrier could also not be ruled-out.

B. ICRF heating performance

During the initial campaign of JET-ILW, fundamental H minority heating in D plasmas was almost exclusively used, with the cyclotron resonance either on-axis or off-axis. Except for specific experiments reported in the previous paragraph, H_2 was injected to establish a H fraction of ~5%. This heating regime when applied on-axis, leads mainly to power deposition on the bulk electrons by collisions with the ICRF-accelerated H ions, and it generally has good single pass wave absorption. The ICRF heating efficiency $\eta = \text{Pabs/Picrf}$, obtained by break-in-slope analysis of the plasma energy response to sharp ICRF power steps[29] was found similar than for JET-C.[30,31] The overall heating performance depends not only of the wave absorption efficiency but also on plasma energy transport and confinement. Figure 10 illustrates the impact of the enhanced radiation from W with the ILW on ICRF performance. The plasma energy achieved per MW of ICRF power is slightly reduced (~20% for L-mode plasmas with central density $\sim 3 \times 10^{19}$ dominantly heated with ~3–4 MW ICRF) with respect to the JET-C, despite the significantly higher bulk radiation level observed with the JET-ILW. For comparison, the radiated power and plasma thermal energy of NBI heated L mode plasmas in JET-ILW and JET-C are plotted in Figure 11. For NBI, the radiated power is also significantly increased with the ILW (although not to the levels of ICRF plasmas) with, as for ICRF, the highest levels of radiation corresponding to lower density plasmas. With the ILW, the thermal energy of the NBI L-mode plasmas is similar than for JET-C. In general, both for ICRF and NBI, the ILW plasmas with lower density and highest radiation tend to have the lowest stored energy. These results are also coherent with the higher thermal energy for pulse 83428 after Be evaporation and with lower radiation as compared to pulse 83383 a reference before Be evaporation (Figure 9(d)). Note that in 83428 a M-mode[28] with enhanced particle confinement developed during the ICRF phase at 10.4 s. ($n_{e,0} = 3 \times 10^{19}\,m^{-3}$ in 83383 and $n_{e,0} = 3.5 \times 10^{19}\,m^{-3}$ in 83428) further enhancing the beneficial effect of reduced radiation on the plasma energy content.

Despite the different heating mechanisms and plasma properties, the plasma heating performance of the NBI and ICRF systems were also found similar.[32,33] This is further illustrated in Figures 12–15. Pulse 81852 is a L-mode plasma ($B_T = 2.55$T, $I_P = 2$MA, $n_{e,0} = 2.4 \times 10^{19}\,m^{-3}$) with a ICRF phase ($f = 42.56$ MHz) and a NBI phase (3.5 MW input power in both cases); Although W and Ni impurity content are larger during RF which explains the larger radiated power in the plasma bulk (1.5 times larger), the plasma thermal energy is similar for both phases. Two important factors

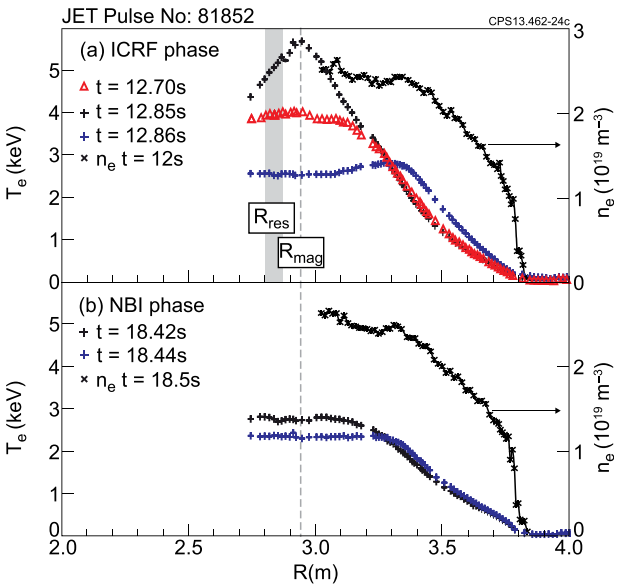

FIG. 14. For pulse 81852, evolution of T_e profiles during sawteeth cycles and n_e profiles (averaged over 1 s), during the ICRF phase (a) and the NBI phase (b). Also shown are the positions of the plasma magnetic axis (R_{mag}) and of the ICRF resonance layer (R_{res}).

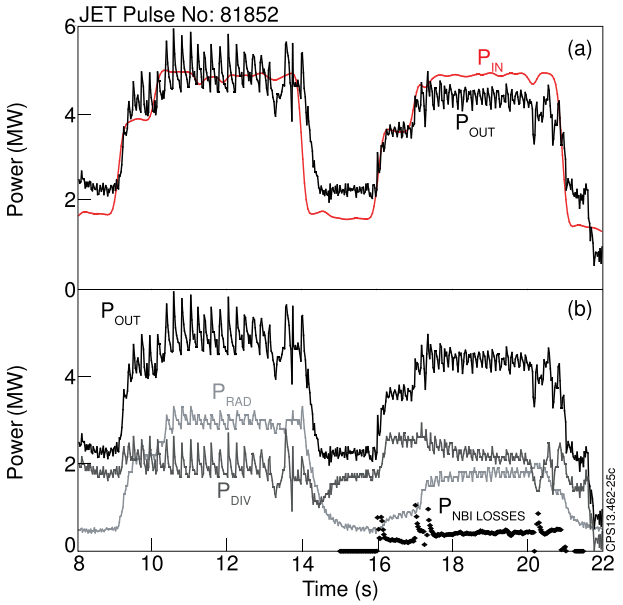

FIG. 15. Power balance for pulse 81852. In (a) P_{IN} the power input to the plasma is compared to P_{OUT}, the power exiting the plasma. P_{IN} includes the ohmic, the ICRF and the NBI power. (b) gives more details on the P_{OUT} accountancy: P_{OUT} includes the total (bulk and divertor region) radiated power, the NBI losses (Shine-through, charge exchange and fast ion orbit losses) and P_{DIV} the power conducted to the divertor.

contribute in preserving the overall ICRF heating performance:

- First, ICRF waves heat efficiently the electrons in the plasma centre as shown from the central electron temperature increase (Figure 12(c)) and from the peaked electron temperature profiles during RF (Figure 14). This results in the higher electron energy content during the ICRF phase (Figure 12(d)). As NBI power is deposited approximately equally on the electrons and on the ions one can speculate that the ion energy compensates during the NBI phase the deficit in electron energy and explain the overall equal thermal energy in the two phases of the pulses but unfortunately Ti measurements were not available for this pulse to confirm this hypothesis.
- Second, plasma radiates power mainly from the outer part as is shown in Figure 13 from bolometric signals and SXR signals analysis. During the RF phase, less than 20% of the total radiated power comes from $\rho < 0.4$ and less than 3% from $\rho < 0.15$.

The power balance for pulse 81852 is illustrated in Figure 15. During the ICRF and NBI heating phases the power input to the plasma ($P_{IN} = P_{ICRF} + P_{NBI} + P_{ohmic}$) and the power exiting the plasma (P_{OUT}) balance well (Figure 15(a)). More details on the accountancy of P_{OUT} are shown in Figure 15(b). $P_{OUT} = P_{RAD} + P_{NBI\_LOSSES} + P_{DIV}$ with the following definitions.

P_{RAD}: total radiated power (from bulk plasma and divertor region) measured with the bolometry diagnostic.

P_{NBI_LOSSES}: NBI power not heating the plasma, including shine-through, charge exchange and fast ion orbit losses estimated using the NUBEAM module[34] in TRANSP.[35]

P_{DIV}: Power conducted to the divertor $P_{DIV} = P_{DIV\_OUTER} + P_{DIV\_INNER}$. P_{DIV_OUTER} is estimated from infra-red thermography of the outer divertor target[36] applying a simple thermal model to deduce the heat-flux from the divertor surface temperature time evolution. The surface temperature of the inner divertor was not measured, and we have assumed $P_{DIV\_OUTER} = 2 \times P_{DIV\_INNER}$.

As could be expected, during the ICRF phase with enhanced plasma radiation the power flux to the divertor is reduced as compared to the NBI phase.

C. Use of ICRF heating in H-mode plasmas

H-mode plasmas with the JET-ILW are prone to W accumulation if reducing the gas dosing too much;[3] indeed, a higher level of gas injection contributes to increase the ELM frequency and reduce the intensity of impurities source. But it also affects the plasma energy confinement.[37] Central electron heating was proved efficient on ASDEX-Upgrade to increase local transport of high Z impurities and prevent accumulation.[38] Although ICRF heating was used in the H-mode plasmas only late in the initial JET-ILW experimental campaign, we have indications that this tool can be used in JET-ILW to prevent impurity accumulation. This is pictured in Figures 16–18 for pulse 83897 ($B_T = 2.65$ T, $I_P = 2$MA, 16.0 MW NBI) and pulse 83603 (same plasma, 14.4 MW NBI and 3.4 MW ICRF heating). Due to the slightly lower NBI power in 83603, the ELM are less frequent before the ICRF phase and impurity flushing by the ELMs at the edge transport barrier is less efficient, hence the increased total radiated power for 83603 at the beginning of the H-mode phase. The central electron temperature (Figures 18(b) and 18(d)) is higher in pulse 83603 thanks to the efficient central electron ICRF heating. In both pulses, infrequent sawteeth are present (~350 ms period in 83597

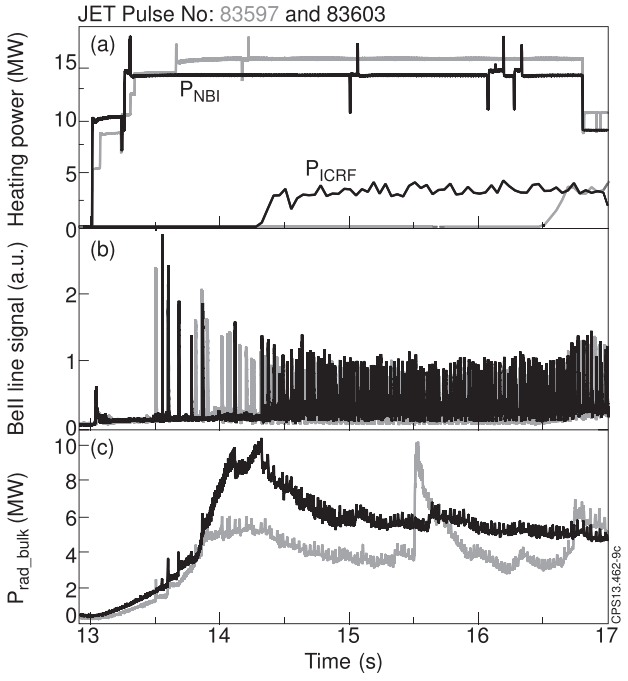

FIG. 16. For pulse 83603 (black) and 83597 (grey) traces of (a) heating power, (b) Be II line emission (ELMs), and (c) bulk radiated power.

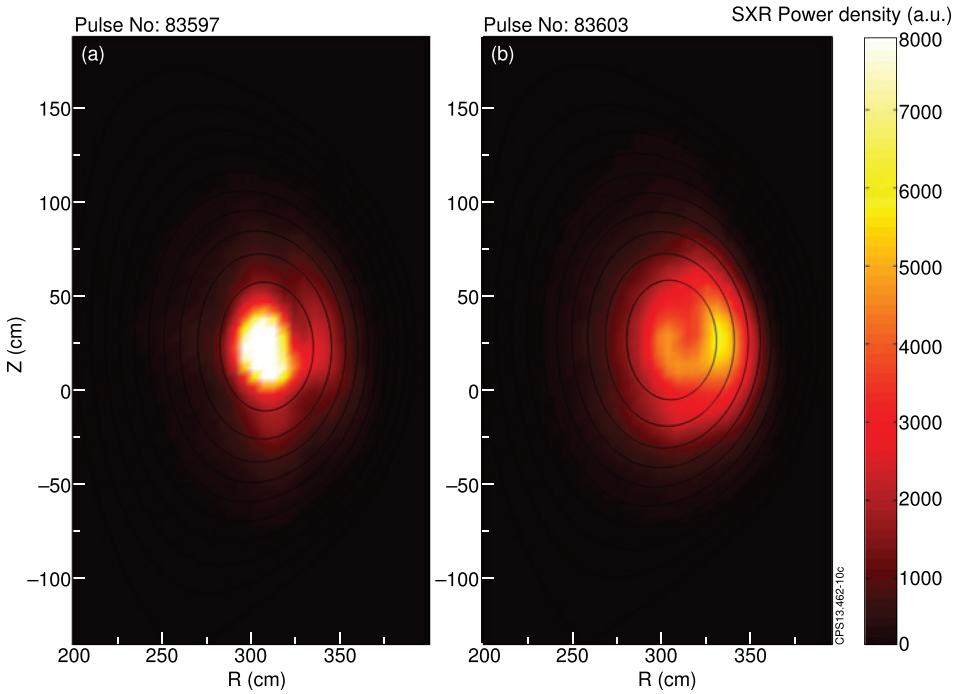

FIG. 17. Tomographic reconstruction of SXR emission right before a sawtooth crash: (a) 83597 (NBI only) t = 15.3151 s, and (b) 83603 (NBI + ICRF) t = 15.3451 s. SXR data are averaged over 10 ms.

and ∼400 ms in 83603). In 83597 the central temperature is decreasing halfway through the sawtooth period, before the crashes, indicating radiating cooling in the plasma centre. This is confirmed by the radiation emission peaked at the centre as measured by bolometry (not shown) and SXR tomography (Figure 17(a)). The tungsten concentration in these plasmas was evaluated from the analysis of SXR emission (see Section II C).[39] The result is shown in Figures 18(a) and 18(c). For the no-RF case, c_W peaks at the centre up to values in the order of 10^{-3}. With ICRF heating in 83603 c_W at mid radius is larger than for NBI heating only, consistent with the overall larger plasma radiation (Figure 16(c)), but tungsten peaking in the center is less pronounced, and c_W at the centre even decreases in the second half of the sawteeth cycles. These results illustrate the potential of central ICRF heating to prevent W accumulation in JET-ILW plasmas.

The possible mechanisms for the reduction of tungsten peaking with ICRF heating in these pulses are discussed in Ref. 40. Central heating could enhance outward neo-classical and anomalous W transport. The observed increased fishbone activity during the pulse with ICRF (during the second half of the sawteeth cycles) which coincides with the reduction of c_W at the centre content also indicates that MHD activity could be an underlying cause for the change of tungsten transport.

IV. CONCLUSIONS

We have characterized operation of the ICRF system during the first experimental campaign with the JET-ILW; the ICRF system operation did not encounter limitations due to the change from the carbon wall to the ILW. The A2 antenna loading is slightly decreased, by at most 20%, with the ILW as compared with JET-C when comparing equivalent plasma conditions. ICRF specific heat fluxes at the antennas are within the JET wall heat handling capabilities. In addition, progresses are being made toward the validation

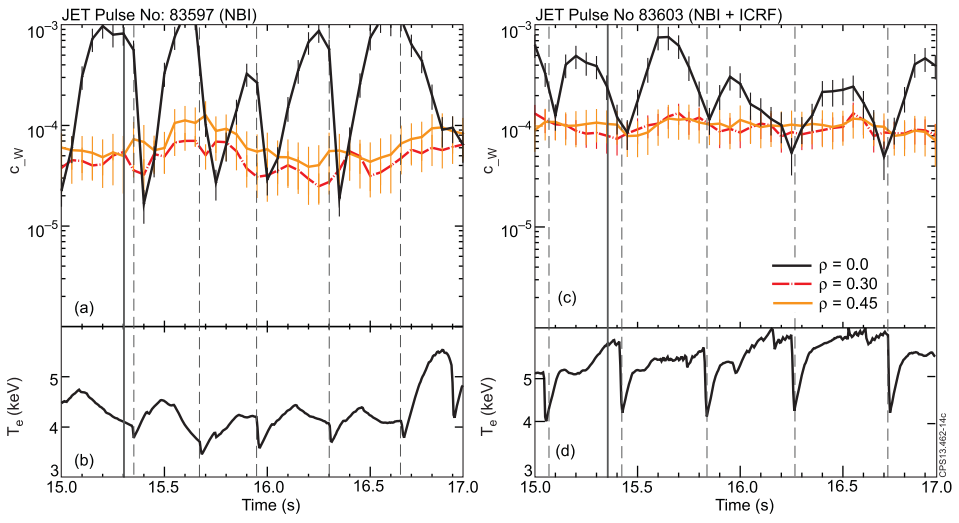

FIG. 18. For pulse 83597 with no ICRF, (a) W concentration estimated from SXR emission profile at normalized radius $\rho = 0.0$, $\rho = 0.3$, and $\rho = 0.45$ and (b) Te at plasma centre. The same quantities are plotted for the pulse 83603 with ICRF in (c) and (d), respectively. The vertical solid lines indicate time when SXR emission profiles are plotted in Figure 17.

of the antenna modeling code TOPICA and of the optimization procedure to reduce the effects of RF sheath rectification in the design of the ITER antenna.

In L-mode, radiation from the JET bulk plasma and impurity levels are higher with ICRF as compared to JET-C, this is attributed to the presence of tungsten in the plasma sputtered from the divertor or other tungsten sources in the JET main chamber. Despite this enhanced radiation with RF, generally ICRF heating has good performance and plasma does not exhibit peaked centre radiation. In addition, we have indications that ICRF central heating is efficient in H-mode plasmas to prevent central W accumulation. In the JET campaign starting in summer 2013, more power will be available in H-mode (straps 3,4 from antenna A and B will be available in the ELM resilient configuration). The emphasis will be on the optimization of the use of ICRF heating to prevent W accumulation, using the ICRF capabilities to provide central electron heating and as a tool for MHD activity control.[41]

ACKNOWLEDGMENTS

The support from the JET ICRH system group is warmly acknowledged. This work, part-funded by the European Communities under the contracts of Association between EURATOM and CCFE, was carried out within the framework of the European Fusion Development Agreement. The views and opinions expressed herein do not necessarily reflect those of the European Commission. This work was also funded by the RCUK Energy Programme under Grant No. EP/I501045.

[1]G. F. Matthews, P. Edwards, T. Hirai, M. Kear, A. Lioure, P. Lomas, A. Loving, C. Lungu, H. Maier, P. Mertens, D. Neilson, R. Neu, J. Pamela, V. Philipps, G. Piazza, V. Riccardo, M. Rubel, C. Ruset, E. Villedieu, and M. Way on behalf of the ITER-like Wall Project Team, Phys. Scr. **T128**, 137–143 (2007).

[2]A. Kaye, T. Brown, V. Bhatnagar, P. Crawley, J. Jacquinot, R. Lobel, J. Plancoulaine, P.-H. Rebut, T. Wade, and C. Walker, Fusion Eng. Des. **24**, 1–21 (1994).

[3]R. Neu, G. Arnoux, M. Beurskens, V. Bobkov, S. Brezinsek, J. Bucalossi, G. Calabro, C. Challis, J. W. Coenen, E. de la Luna, P. C. de Vries, R. Dux, L. Frassinetti, C. Giroud, M. Groth, J. Hobirk, E. Joffrin, P. Lang, M. Lehnen, E. Lerche, T. Loarer, P. Lomas, G. Maddison, C. Maggi, G. Matthews, S. Marsen, M.-L. Mayoral, A. Meigs, Ph. Mertens, I. Nunes, V. Philipps, T. Pütterich, F. Rimini, M. Sertoli, B. Sieglin, A. C. C. Sips, D. van Eester, G. van Rooij, and JET-EFDA Contributors, Phys. Plasmas **20**, 056111 (2013).

[4]M.-L. Mayoral, V. Bobkov, A. Czarnecka, I. Day, A. Ekedahl, P. Jacquet, M. Goniche, R. King, K. Kirov, E. Lerche, J. Mailloux, D. Van Eester, O. Asunta, C. Challis, D. Ciric, J. W. Coenen, L. Colas, M. C. Giroud, M. Graham, I. Jenkins, E. Joffrin, T. Jones, D. King, V. Kiptily, C. C. Klepper, C. Maggi, F. Marcotte, G. Matthews, D. Milanesio, I. Monakhov, M. Nightingale, R. Neu, J. Ongena, T. Pütterich, V. Riccardo, F. Rimini, J. Strachan, E. Surrey, V. Thompson, G. Van Rooij, and JET EFDA contributors, "On the challenge of plasma heating with the JET metallic wall," in *Proceedings of 24th IAEA Fusion Energy Conference* (San Diego, USA, 2012), p. EX/4-3.

[5]M. Graham, M.-L. Mayoral, I. Monakhov, J. Ongena, T. Blackman, M. P. S. Nightingale, E. Wooldridge, F. Durodié, A. Argouarch, G. Berger-By, A. Czarnecka, S. Dowson, R. Goulding, S. Huygen, P. Jacquet, T. J. Wade, E. Lerche, P. U. Lamalle, H. Sheikh, D. Van Eester, M. Vrancken, A. Walden, A. Whitehurst, and JET-EFDA contributors, Plasma Phys. Controlled Fusion **54**, 074011 (2012).

[6]I. Monakhov, M. Graham, T. Blackman, S. Dowson, F. Durodie, P. Jacquet, J. Lehmann, M.-L. Mayoral, M. P. S. Nightingale, C. Noble, H. Sheikh, M. Vrancken, A. Walden, A. Whitehurst, E. Wooldridge, and JET-EFDA Contributors, Nucl. Fusion **53**, 083013 (2013).

[7]D. Milanesio, O. Meneghini, V. Lancellotti, R. Maggiora, and G. Vecchi, Nucl. Fusion **49**, 115019 (2009).

[8]F. Durodie, M. Vrancken, R. Bamber, P. Dumortier, D. Hancock, S. Huygen, D. Lockley, F. Louche, R. Maggiora, D. Milanesio, A. Messiaen, M. P. S. Nightingale, M. Shannon, P. Tigwell, M. Van Schoor, D. Wilson, K. Winkler, and CYCLE Team, "RF optimization of the port plug layout and performance assessment of the ITER ICRF antenna," in *Proceedings of the 24th IAEA Fusion Energy Conference* (San Diego, USA, 2012), p. ITR/P1-08.

[9]R. Bilato, M. Brambilla, D. A. Hartmann, and A. Parisot, Nucl. Fusion **45**, L5–7 (2005).

[10]M. Groth, S. Brezinsek, P. Belo, M. N. A. Beurskens, M. Brix, M. Clever, J. W. Coenen, C. Corrigan, T. Eich, J. Flanagan, C. Guillemaut, C. Giroud, D. Harting, A. Huber, S. Jachmich, U. Kruezi, K. D. Lawson, M. Lehnen, C. Lowry, C. F. Maggi, S. Marsen, A. G. Meigs, R. A. Pitts, G. Sergienko, B. Sieglin, C. Silva, A. Sirinelli, M. F. Stamp, G. J. van Rooij, S. Wiesen, and JET-EFDA Contributors, Nucl. Fusion **53**, 093016 (2013).

[11]P. Jacquet, V. Bobkov, M.-L. Mayoral, I. Monakhov, J. M. Noterdaeme, A. Scarabosio, I. Stepanov, M. Vrancken, E. Wolfrum, and ASDEX Upgrade Team, Nucl. Fusion **52**, 042002 (2012).

[12]M.-L. Mayoral, V. Bobkov, L. Colas, M. Goniche, J. Hosea, J. G. Kwak, R. Pinsker, S. Moriyama, S. Wukitch, F. W. Baity, S. Carpentier-Chouchana, A. Czarnecka, A. Ekedahl, G. Hanson, P. Jacquet, P. Lamalle, I. Monakhov, M. Murakami, A. Nagy, M. Nightingale, J.-M. Noterdaeme, J. Ongena, P. M. Ryan, M. Vrancken, J. R. Wilson, EFDA–JET contributors, ASDEX Upgrade Team, and the ITPA "Integrated Operation Scenarios" members and experts, "On maximizing the ICRF antenna loading for ITER plasmas," in *Proceedings of the 23rd IAEA Fusion Energy Conference* (2010), pp. ITR/P1-11, see http://www-naweb.iaea.org/napc/physics/FEC/FEC2010/html/node54.htm.

[13]P. Jacquet, L. Colas, M.-L. Mayoral, G. Arnoux, V. Bobkov, M. Brix, P. Coad, A. Czarnecka, D. Dodt, F. Durodie, A. Ekedahl, D. Frigione, M. Fursdon, E. Gauthier, M. Goniche, M. Graham, E. Joffrin, A. Korotkov, E. Lerche, J. Mailloux, I. Monakhov, C. Noble, J. Ongena, V. Petrzilka, C. Portafaix, F. Rimini, A. Sirinelli, V. Riccardo, Z. Vizvary, A. Widdowson, K.-D. Zastrow, and JET EFDA Contributors, Nucl. Fusion **51**, 103018 (2011).

[14]P. Jacquet, F. Marcotte, L. Colas, G. Arnoux, V. Bobkov, Y. Corre, S. Devaux, J.-L. Gardarein, E. Gauthier, M. Graham, E. Lerche, M.-L. Mayoral, I. Monakhov, F. Rimini, A. Sirinelli, D. Van Eester, and JET EFDA contributors, J. Nucl. Mater. **438**, S379–S383 (2013).

[15]J. Jacquot, D. Milanesio, L. Colas, Y. Corre, M. Goniche, J. Gunn, S. Heuraux, and M. Kubič, Phys. Plasmas **21**, 061509 (2014).

[16]A.-L. Campergue, P. Jacquet, V. Bobkov, D. Milanesio, I. Monakhov, L. Colas, G. Arnoux, M. Brix, A. Sirinelli, and JET-EFDA Contributors, AIP Conf. Proc. **1580**, 263 (2014).

[17]L. Colas, D. Milanesio, E. Faudot, M. Goniche, and A. Loarte, J. Nucl. Mater. **390–391**, 959–962 (2009).

[18]L. L. Lao, J. R. Ferron, R. J. Groebner, W. Howl, H. St. John, E. J. Strait, and T. S. Taylor, Nucl. Fusion **30**, 1035 (1990).

[19]M. Becoulet, L. Colas, S. Pecoul, J. Gunn, Ph. Ghendrih, A. Becoulet, and S. Heuraux, Phys. Plasmas **9**, 2619–2632 (2002).

[20]A. Czarnecka, F. Durodié, A. C. A. Figueiredo, K. D. Lawson, E. Lerche, M.-L. Mayoral, J. Ongena, D. Van Eester, K.-D. Zastrow, Vl. V. Bobkov, I. H. Coffey, L. Colas, P. Jacquet, I. Monakhov, and JET-EFDA contributors, Plasma Phys. Controlled Fusion **54**, 074013 (2012).

[21]T. Pütterich, R. Dux, M. N. A. Beurskens, V. Bobkov, S. Brezinsek, J. Bucalossi, J. W. Coenen, I. Coffey, A. Czarnecka, C. Giroud, E. Joffrin, K. D. Lawson, M. Lehnen, E. de la Luna, J. Mailloux, S. Marsen, M.-L. Mayoral, A. Meigs, R. Neu, F. Rimini, M. Sertoli, M. Stamp, G. van Rooij, and JET EFDA Contributors, "Tungsten screening and impurity control in JET," in *Proceedings of 24th IAEA Fusion Energy Conference* (San Diego, USA, 2012), pp. EX/P3–15.

[22]A. Czarnecka, V. Bobkov, I. H. Coffey, L. Colas, P. Jacquet, K. D. Lawson, E. Lerche, C. Maggi, M.-L. Mayoral, T. Pütterich, D. Van Eester, and JET-EFDA Contributors, AIP Conf. Proc. **1580**, 227 (2014).

[23]D. Kalupin, I. Ivanova-Stanik, I. Voitsekhovitch, J. Ferreira, D. Coster, L. L. Alves, Th. Aniel, J. F. Artaud, V. Basiuk, J. P. S. Bizarro, R. Coelho, A. Czarnecka, Ph. Huynh, A. Figueiredo, J. Garcia, L. Garzotti, F. Imbeaux, F. Köchl, M. F. Nave, G. Pereverzev, O. Sauter, B. D. Scott,

R. Stankiewicz, P. Strand, ITM-TF Contributors, and JET-EFDA Contributors, Nucl. Fusion **53**, 123007 (2013).
[24]Vl. Bobkov, G. Arnoux, S. Brezinsek, J. W. Coenen, L. Colas, M. Clever, A. Czarnecka, F. Braun, R. Dux, A. Huber, P. Jacquet, C. Klepper, E. Lerche, C. Maggi, F. Marcotte, M. Maslov, G. Matthews, M. L. Mayoral, K. McCormick, A. Meigs, D. Milanesio, I. Monakhov, R. Neu, J.-M. Noterdaeme, Th. Pütterich, F. Rimini, G. Van Rooj, G. Sergienko, D. Van Eester, and JET EFDA Contributors, J. Nucl. Mater. **438**, S160–S165 (2013).
[25]C. C. Klepper, P. Jacquet, V. Bobkov, L. Colas, T. M. Biewer, D. Borodin, A. Czarnecka, C. Giroud, E. Lerche, V. Martin, M.-L. Mayoral, F. Rimini, G. Sergienko, D. Van Eester, and JET EFDA Contributors, J. Nucl. Mater. **438**, S594–S598 (2013).
[26]A. G. Meigs, S. Brezinsek, M. Clever, A. Huber, S. Marsen, C. Nicholas, M. Stamp, K.-D. Zastrow, and JET EFDA Contributors, J. Nucl. Mater. **438**, S607–S611 (2013).
[27]D. Van Eester, E. Lerche, P. Jacquet, V. Bobkov, A. Czarnecka, J. W. Coenen, L. Colas, K. Crombé, M. Graham, S. Jachmich, E. Joffrin, C. C. Klepper, V. Kiptily, M. Lehnen, C. Maggi, F. Marcotte, G. Matthews, M.-L. Mayoral, K. Mc Cormick, I. Monakhov, M. F. F. Nave, R. Neu, C. Noble, J. Ongena, T. Pütterich, F. Rimini, E. R. Solano, G. van Rooij, and JET-EFDA Contributors, AIP Conf. Proc. **1580**, 223 (2014).
[28]E. R. Solano, F. Rimini, B. Alper, P. Belo, A. Boboc, M. Brix, A. Figueiredo, L. Frassinetti, S. Gerasimov, D. Howell, C. Maggi, K. McCormick, I. Nunes, S. Pinches, D. Refy, B. Sieglin, and JET EFDA Contributors, "M-mode: axi-symmetric magnetic oscillation and ELM-less H-mode in JET," in *Proceedings of the 39th EPS Conference and 16th International Congress on Plasma Physics* (2012), p. P2.060.
[29]E. A. Lerche, D. Van Eester, and JET EFDA contributors, Plasma Phys. Controlled Fusion **50**, 035003 (2008).
[30]D. Van Eester, E. Lerche, P. Jacquet, V. Bobkov, A. Czarnecka, J. W. Coenen, L. Colas, K. Crombé, M. Graham, S. Jachmich, E. Joffrin, C. C. Klepper, F. Marcotte, M.-L. Mayoral, I. Monakhov, F. Nave, J. Ongena, T. Pütterich, F. Rimini, G. van Rooij, and JET-EFDA Contributors, "Characterization of ion cyclotron resonance heating in presence of the ITER-like wall in JET," in *Proceedings of the 39th EPS Conference and 16th International Congress on Plasma Physics* (2012), p. P1.094.
[31]E. Lerche, D. Van Eester, P. Jacquet, M.-L. Mayoral, V. Bobkov, L. Colas, A. Czarnecka, K. Crombé, I. Monakhov, F. Rimini, M. Santala, and JET-EFDA Contributors, Nucl. Fusion **54**, 073006 (2014).
[32]E. Lerche, D. Van Eester, Ph. Jacquet, M.-L. Mayoral, V. Bobkov, L. Colas, A. Czarnecka, M. Graham, G. Matthews, I. Monakhov, R. Neu, T. Puetterich, F. Rimini, P. de Vries, and JET-EFDA Contributors, AIP Conf. Proc. **1580**, 235 (2014).
[33]M.-L. Mayoral, T. Pütterich, P. Jacquet, E. Lerche, D. Van-Eester, V. Bobkov, C. Bourdelle, L. Colas, A. Czarnecka, J. Mlynar, R. Neu, and JET-EFDA Contributors, AIP Conf. Proc. **1580**, 231 (2014).
[34]A. Pankin, D. McCune, R. Andre, G. Bateman, and A. Kritz, Comput. Phys. Commun. **159**, 157–184 (2004).
[35]R. J. Goldston, D. C. McCune, H. H. Towner, S. L. Davis, R. J. Hawryluk, and G. L. Schmidt, J. Comput. Phys. **43**, 61 (1981).
[36]I. Balboa, G. Arnoux, T. Eich, B. Sieglin, S. Devaux, W. Zeidner, C. Morlock, U. Kruezi, G. Sergienko, D. Kinna, P. D. Thomas, M. Rack, and JET EFDA Contributors, Rev. Sci. Instrum. **83**, 10D530 (2012).
[37]G. Saibene, L. D. Horton, R. Sartori, B. Balet, S. Clement, G. D. Conway, J. G. Cordey, H. P. L. De Esch, L. C. Ingesson, J. Lingertat, R. D. Monk, V. V. Parail, R. J. Smith, A. Taroni, K. Thomsen, and M. G. von Hellermann, Nucl. Fusion **39**, 1133–1156 (1999).
[38]C. Angioni, L. Carraro, T. Dannert, N. Dubuit, R. Dux, C. Fuchs, X. Garbet, L. Garzotti, C. Giroud, R. Guirlet, F. Jenko, O. J. W. F. Kardaun, L. Lauro-Taroni, P. Mantica, M. Maslov, V. Naulin, R. Neu, A. G. Peeters, G. Pereverzev, M. E. Puiatti, T. Pütterich, J. Stober, M. Valovič, M. Valisa, H. Weisen, A. Zabolotsky, ASDEX Upgrade Team, and JET EFDA Contributors, Phys. Plasmas **14**, 055905 (2007).
[39]T. Pütterich, R. Dux, R. Neu, M. Bernert, M. N. A. Beurskens, V. Bobkov, S. Brezinsek, C. Challis, J. W. Coenen, I. Coffey, A. Czarnecka, C. Giroud, A. Gude, E. Joffrin, A. Kallenbach, M. Lehnen, E. Lerche, E. de la Luna, S. Marsen, G. Matthews, M.-L. Mayoral, R. M. McDermott, A. Meigs, M. Sertoli, G. van Rooij, J. Schweinzer, ASDEX Upgrade Team, and JET EFDA Contributors, "Taming Tungsten in JET and ASDEX Upgrade," in 40th EPS conference on Plasma Physics, Espoo, Finland, 2013.
[40]T. Pütterich, R. Dux, R. Neu, M. Bernert, M. N. A. Beurskens, V. Bobkov, S. Brezinsek, C. Challis, J. W. Coenen, I. Coffey, A. Czarnecka, C. Giroud, P. Jacquet, E. Joffrin, A. Kallenbach, M. Lehnen, E. Lerche, E. de la Luna, S. Marsen, G. Matthews, M.-L. Mayoral, R. M. McDermott, A. Meigs, J. Mlynar, M. Sertoli, G. van Rooij, ASDEX Upgrade Team, and JET EFDA Contributors, Plasma Phys. Controlled Fusion **55**, 124036 (2013).
[41]J. P. Graves, I. T. Chapman, S. Coda, M. Lennholm, M. Albergante, and M. Jucker, Nature Commun. **3**, 624 (2012).